

Exploring the Borderland between Physics and Chemistry: Theoretical Methods in the Study of Atomic Clusters

Yamil Simón-Manso^a, Carlos Gonzalez^b and Patricio Fuentealba^c

Experimental and theoretical studies of atomic clusters have proven to be a challenging research theme, but also one of great practical importance in developing new technologies [1 and references therein]. The physical and chemical properties of atomic clusters lie between the properties of molecular systems and solids and are often unique. This article describes a number of theoretical methodologies currently applied to study small atomic clusters. Several current methods for optimizing cluster geometries, such as genetic algorithm, simulated annealing and the big bang method are described and illustrated. We discuss the theoretical tools used in cluster studies to describe the chemical bonding and to predict chemical reactivity. In particular, we emphasize the use of the Electron Localization Function (ELF) and the Fukui function for these purposes. We also include a brief discussion of recent reports of unusual physical properties of metallic clusters and the application of Density Functional Theory methods to shed light on the physics of these phenomena. Of special interest is magnetism observed in clusters and films of gold, a typically diamagnetic metal.

^a Chemical and Biochemical Reference Data Division, National Institute of Standards and Technology, 100 Bureau Drive, M/S 8320, Gaithersburg, MD 20899. Phone: (301) 975-8638. E-mail: ysimon@nist.gov.

^b Chemical and Biochemical Reference Data Division, National Institute of Standards and Technology, 100 Bureau Drive, M/S 8320, Gaithersburg, MD 20899. Phone: (301) 975-2483. E-mail: carlos.gonzalez@nist.gov.

^c Facultad de Ciencias, Departamento de Física, Universidad de Chile, Casilla 653, Santiago, Chile. Phone: (56 2) 978 7268. E-mail: pfuentealba@uchile.cl.

1. Introduction

In recent times, there have been many investigations that lie at the border between physics and chemistry. It is not new to these sciences; it has happened in the past with many other disciplines, such as the kinetic theory of gases, low temperature studies, theory of solutions, the study of physical properties of compounds, molecular structure studies [2, and references therein]. There is invariably a great deal of work that must be done before disciplines at the frontier of two sciences become an integral part of one another. The experimental and theoretical study of atomic clusters is a modern discipline that lies between physics and chemistry. It is a discipline in the making; simply finding an unambiguous definition of atomic clusters is a difficult task.

Most researchers 'define' a cluster similar to the definition given by Connerade et al. [3], "a group of atoms (structural sub-units) bound together by interatomic forces is called a cluster. There is no qualitative distinction between small clusters and molecules, except perhaps that the binding forces must be such as to permit the molecule (system) to grow much larger by stacking more atoms or molecules (sub-units) of the same type if the system is to be called a cluster." It is worth mentioning that from the chemist's perspective, any arrangement of atoms without a covalent bond should not be considered a molecule. A typical covalent bond implies binding energies greater than 15 kcal/mol and bond distances smaller than 2.0 Å. In fact, the nature of chemical bonding in clusters can vary strongly. For instance, magnesium dimer is a van der Waals system, as are Mg_3 and Mg_4 . Magnesium clusters with more than ten atoms are more covalent in nature and the largest clusters at some point should experience a transition to metallic bonding characteristic of a solid. In reality, the binding forces in atomic clusters may be metallic, covalent, ionic, hydrogen-bonded or van der Waals in character.

The structural and compositional diversity of clusters is huge. All the units (components) of a cluster are not necessarily atoms or monatomic ions. For example, a cluster may be an arrangement of a metal core with one or several atoms surrounded by molecules, so-called ligands, or may be exclusively formed by molecules. It should be noted that ligands play a stabilizing role in chemically synthesized metal clusters and consequently ligands substantially modify the physical and chemical properties of the clusters. Throughout this article we shall refer to bare clusters (atomic clusters) with a single component, unless otherwise stated. The properties of the atomic clusters can vary from atomic to bulk properties, but are also often unique depending on their size and elemental composition. Many clusters with sizes in the range of nanoparticles, between 1 and 100 nm, and thin films have shown unexpected properties and have found use in areas such as catalysis and magnetic storage [1, 4, 5].

The presence of dangling bonds (unsatisfied valences) on the surface makes clusters chemically very active. In general, clusters may split or combine with other particles more rapidly than normal molecules. This means that they are much more reactive, and therefore, more difficult to stabilize for study in the laboratory with conventional methods. Hence, most experimental measurements are carried out in the gas phase at low pressures and require sophisticated instrumentation. Experimental difficulties are one of the main reasons that theoretical work on clusters is so valuable. As an added benefit, research in this field has united chemists and physicists, both experimental and theoretical, to study a huge variety of phenomena in a very detailed and synergistic manner. One of the first successful attempts to rationalize an experimental observation of cluster phenomena was the explanation of the existence of magic numbers in the abundance spectrum of alkali metal clusters [6], which was concurrently explained by the very simple theoretical jellium model [7, 8]. Magic numbers arise as a consequence of filling molecular orbitals to form a closed shell species like the atomic noble gases, giving them extra stabilization energy with a large HOMO-LUMO gap. However, it was also realized early on that to explain the variation of most of the properties of a given cluster with respect to the number of atoms, it is necessary to use theoretical models that take into account the quantum nature of the electronic

structure [9]. Fortunately, around the same time Density Functional Theory (DFT) emerged as a robust and efficient methodology to perform calculations of the electronic structure of atoms, molecules and clusters of moderate size [10-11].

We briefly discuss some key steps that most researchers perform in conducting theoretical studies of atomic clusters. This article does not provide a systematic study (or review) of this topic, but a short description of our own and related research. It is set out in five sections, beginning with this introduction. In the second section, we use DFT calculations to describe clusters as entities that lie between atoms and solids with unique properties depending on their size, chemical nature and symmetry. The third section describes several methods of finding different stable isomers of a given cluster. There are various stochastic methodologies and evolutionary algorithms currently used for this task; we shall discuss the genetic algorithm, simulated annealing and the so-called “big bang” methods. The chemical bonding and reactivity of clusters are discussed in section 4. We present the electron localization function (ELF) as a very robust tool to understand chemical bonding in clusters and the Fukui function as an effective means of predicting their chemical reactivity. Finally, in section 5 we discuss some interesting properties of clusters such as the magnetic moment observed in clusters and surfaces of gold, a typically diamagnetic metal, from a theoretical point of view.

2. Clusters: Between Atoms and Bulk

Recently, the study – both experimental and theoretical – of the transition from atomic and molecular clusters to bulk solids has become accessible for almost any type of material. Atomic clusters represent an intermediate state between molecules and bulk solids and are very useful as models of nanoparticles, surfaces or solids to study phenomena such as physical adsorption, chemisorption, plasmon excitations and magnetism. However, this modeling might be incomplete or even incorrect due to the fact that the electronic properties of clusters change dramatically with size and frequently experience many transitions such as metal-insulator, color absorption and collective excitations [3, and references therein]. The fact that the chemical and physical properties of clusters do not change monotonically with their sizes complicates the exploration of trends and applications in this area. Most cluster properties show great fluctuations and very irregular dependence on size. Even so, the mean nearest-neighbour coordination numbers vary with the cluster sizes, thus the cluster properties shift gradually from surface-dominated to volume-dominated.

Estimating the number of atoms that are needed in a cluster to mimic a nanoparticle, an infinite surface or the bulk solid is an important part of modeling atomic clusters. However, other factors need to be considered for proper modeling. Frequently it is necessary to impose additional constraints on the models to avoid unphysical situations. For example, in theoretical calculations where the cluster is intended to represent the bulk or a bulk region, it should be subjected to crystal symmetry constraints [12]. The crystal symmetry determines the symmetry of the band structure due to the commutation between symmetry operations and the crystal Hamiltonian [13]. Fully optimized cluster geometries frequently deviate from the bulk symmetry yielding substantial differences in most of the calculated cluster properties. Also, many small clusters experience spontaneous symmetry-breaking events, such as Pierls' distortions (Jahn-Teller effect), that must be considered [14]. In magnetic systems, certain restrictions on the spin symmetry may be

necessary [15]. Although the complete theoretical description of a quantum many-body problem, even of moderate size (less than one hundred atoms), is very difficult, DFT is able to deliver reliable results in many cluster problems. DFT is possibly the only *ab initio* correlated method that can be implemented and used with reasonable computational cost for describing the electronic structure of molecular systems and solids.

In Figure 1 we show the binding energy per atom (BE) dependence on the cluster size (N) of a representative metal (lithium) and a transition metal (Cu). Binding energies are calculated using

$$BE = \frac{E[cluster] - N E[atom]}{N} \quad (1)$$

where BE , E and N stand for binding energy, total energy and number of atoms, respectively. The all-electron calculations were done at the BP86/6-31G(d) level of theory, which implies use of a DFT electronic structure method with Becke's 1988 exchange functional [16] and Perdew's gradient-corrected correlation functional method (BP86) [17] in conjunction with the Pople basis set 6-31G with an additional set of polarization d-functions added to all nonhydrogen atoms [18]. The clusters used in this calculation are portions of the fcc-structure centered on one atom with the highest possible symmetry beginning with the tetrahedron and successively adding atoms to form new tetrahedrons. For example, 12 atoms surrounding the reference atom complete the first-neighbor shell. The bond distances are fixed to the values of the bulk metals, 2.56 Å for copper and 3.11 Å for lithium. The calculated binding energies change smoothly with cluster size when the models are constrained to the crystal symmetry (or a subgroup) and reach saturation values that depend on the nature of the metal. As shown in Figure 1, the binding energy per atom in the case of lithium clusters levels-off more quickly than in the case of copper because alkali metals have energy bands very similar to those of free electrons [13]. The saturation values of the binding energies found by polynomial extrapolation differ by 8–10 kcal/mole from the bulk values of approximately 29 kcal/mol for lithium and 80 kcal/mol for copper [19], but most of these differences are attributable to basis set superposition error and a small part is due to an embedded effect that can be corrected with an external potential with the crystal symmetry [12,

20]. The fluctuations of the second finite differences of the BE vs. N dependence ($\Delta^2 E / \Delta N^2$) are very small, and only the smallest clusters (4 and 6 atoms) show significant deviations, according with their lower symmetry.

We also have explored some properties (not shown in the figure), such as ionization potentials, electron affinities, and HOMO-LUMO gaps with similar results [12]. It is worth mentioning that the number of atoms needed to reach the saturation values depends on the property itself and not only on the nature of the metal.

In summary, a general cluster model should contain at least the minimum number of atoms to represent the set of properties to be studied. According to our calculations, a lower bound to the critical cluster size necessary to represent bulk properties and transitions depends on the nature of the metal and crystal symmetry and should always be tested against reliable experimental values. At the same time, these calculations reveal that the fluctuations observed in the size-dependent cluster properties are due to the fact that actual cluster does not preserve the full symmetry of the crystal. Most clusters, regardless the experimental technique used to create them, suffer dynamic rearrangements leading to more stable structures. Thus, an important part of all cluster studies is to find the optimum structures in the configuration space spanned by the nuclear coordinates. Below we discuss some of the most common methods used to optimize the geometry of clusters.

3. Optimization methods applied to cluster studies. Finding the most stable isomers

In general terms, the problem of finding stable isomer structures is equivalent to the problem of finding minima on a multi-dimensional hypersurface. Every local minimum represents the geometry of an isomer and the global minimum is the most stable one (i.e. the geometry with the lowest total energy). The total energy is a function of the nuclear coordinates. There are $3N-6$ variables ($3N-5$ in the case of a linear molecule), where N is the number of atoms. In general, geometry optimization is a non-trivial mathematical problem that does not lend itself to an analytic solution. Therefore, it is necessary to use numerical techniques. There are two main types of optimization techniques, those that follow the gradient (of the total energy) to reach a minimum energy and stochastic techniques. (Recently some very interesting techniques based on quantum molecular dynamics have emerged, but these will not be addressed here [21].) The most traditional methods used in quantum chemistry are gradient-following techniques and are implemented in almost all computational codes. The most successful gradient-following techniques are approximations to Newton's method and are termed quasi-Newton methods. These need a very limited number of energy and gradient evaluations compared to other approaches and are therefore very efficient. However, they are dependent on the initial geometry and locate only one stationary point at a time. They cannot jump from one minimum to another. Hence, if one has a good initial guess of the geometry of the most stable isomer, a quasi-Newton optimization is likely the most effective method. Nevertheless, one cannot be sure to have reached the global minimum. In the case of an optimization of "normal" molecules, where the chemical bonding rules reliably predict the geometry of the most stable isomer, quasi-Newton methods are very useful. However, for a cluster with a moderate number of atoms, for instance Si_9 , the chemical rules of bonding are not as helpful and the number of isomers with energies close to the global minimum energy is high. For Si_9 there are at least 14 such isomers [22].

On the other hand, stochastic methods are based on a random search on the potential energy hypersurface (PEH). As a consequence, they are able to jump from one minimum to another,

allowing the location of various isomers in one run. They are also, in principle, independent of the initial guess. However, this should be verified by performing a series of similar optimizations starting at different locations on the PEH of the system under study. The drawback of stochastic methods is that they generally need many more evaluations of the energy function than quasi-Newton methods, which makes it difficult to apply them at a high level of electronic structure theory. Usually, one starts with a low level, in many cases classical molecular dynamics, and then proceeds to perform high-level calculations of the minima identified at the lower level. There are a variety of stochastic methodologies, and each has several variants. We will briefly describe three of them: genetic algorithm, simulated annealing and the big bang method.

Genetic Algorithm

Genetic Algorithm techniques are based on the ideas of Darwinian biological evolution, and have recently been widely used in the optimization of atomic clusters [23, 24]. One starts by defining a *genome* or string that represents a candidate solution to the problem. In the case of atomic clusters, the choice is simple: the genome is a set of coordinates for each atom of the cluster. One starts with an initial population of genomes selected randomly. This population will be propagated to produce more “fit” species by applying “natural selection” rules; in the case of clusters this means combining clusters with low energies to (hopefully) produce new cluster geometries which lead to still lower cluster energies. In order to increase sampling of the search space, one defines operators simulating crossover and mutation and applies these to the developing population. The lowest energy clusters are produced based on the principle of “survival of the fittest.” At each step, population members with energy above a given threshold are deleted from the population, and species with low energies are allowed to reproduce. In this way, after a given number of generations, one should obtain structures of lower energy. In the case of clusters, this means low-lying isomers.

The initial population of individuals, represented as a set of atomic coordinates, is generated randomly. In practice, different constraints can be imposed to avoid searching very unphysical

regions of the hypersurface. The coordinates should be constrained to lie inside a box of the expected dimensions of the cluster, and any pair of atoms can neither be closer than a given distance nor separated by more than a given distance. The specific criteria for desired fitness, selection rules and crossover and mutation probabilities are specific to every genetic algorithm implementation. In this part of the work, we followed the algorithm presented in Ref. [25]. The number of times one needs to evaluate the energy can become significantly large. Therefore, it is common practice to produce all generations in the genetic algorithm cycles using an empirical molecular orbital method, such as MSINDO [26]. It is also important to note that each individual is an optimized geometry within the semiempirical method. When the genetic algorithm optimization is complete, the resulting isomers are re-optimized using a high-level electronic structure theory, usually Kohn-Sham DFT including an exchange correlation functional via a conventional gradient-following quasi-Newton optimization technique.

As an example, in Ref. [22] the genetic algorithm was used to find fourteen isomers of the Si_9 cluster. The eight most important isomer structures are presented in Fig. 2. All of the structures were optimized using the B3PW91 functional with the Stuttgart pseudopotential [27]. Since the corresponding basis set does not contain diffuse and polarization functions, the basis was augmented with diffuse s- and p-functions and one set of d-polarization function from the Sadlej basis set [28]. To ensure that the optimized structures are stationary points on the molecular potential energy surface, vibrational frequencies were calculated and found to be positive indicating a minimum geometry. The structures are given in Fig. 2 in order of increasing energy. Some of the properties of these clusters are displayed in Table 1. One can see that there is less than a 0.23 eV difference in the binding energy per atom between the first and the last isomer. The binding energy per atom correlates reasonably well with the energy of the HOMO. However, there does not seem to be any correlation with the dipole polarizability or with the HOMO-LUMO gap [22].

Using the same methodology as in Ref. [29], the following larger silicon clusters were studied: Si₄₀, Si₄₆ and Si₆₀ (the last one was included in this study due to its possible similarity to C₆₀). Figure 3 shows the four most stable isomers of Si₆₀. Structure (b) corresponds to the structure reported in Ref. [30]. However, the calculations of Ref. [29] show that at this level of theory, the structure has five imaginary frequencies. All of the structures in Fig. 3 are very close in binding energy making it difficult to predict the most stable isomer. However, it is clear that for the Si₆₀ cluster there is no cage structure similar to the fullerene structure observed for carbon atom clusters. In addition, it is observed that the silicon cluster structures are more prolate in shape than their carbon counterparts.

As discussed in Ref. [29], one significant weakness of the methodology consists of the use of a semiempirical method, MSINDO, to evaluate the atomic clusters. For example, silicon clusters of the endohedral type, where some silicon atoms are hypervalent, are not properly described given that the semiempirical methodology is not parametrized to treat hypervalent silicon atoms.

Simulated Annealing


In this subsection we discuss simulated annealing techniques [31, 32] as implemented by Perez et al. [33]. In this methodology the system is allowed to evolve inside a box of a given length. The method is initialized with randomly selected cluster geometries and the energy of each atomic cluster is calculated using some quantum chemical method. In this case, the energy is evaluated at each step at the HF/Lanl2z level of theory. Every generated structure is then subject to one or more acceptance tests. If the energy is lowered, $\Delta E \leq 0$, the new structure is accepted;

otherwise, if $\Delta E > 0$, the structure is accepted if $\Phi(\Delta E) < P(\Delta E)$, where

$P(\Delta E) = \exp(-\Delta E/k_B T)$ is the Boltzmann probability distribution function and

$\Phi(\Delta E) = |\Delta E/E_j|$ where E_j is the energy of the structure being evaluated. (Most simulated

annealing algorithms are based on the Metropolis sampling method that simply compares

 to a random number between 0 and 1.) If neither test is satisfied, the new structure is not

accepted, the parent structure is subjected to another random modification, and the acceptance procedure is repeated. At every temperature there is a maximum number of generated structures that satisfy neither of the two acceptance criteria. This number is reduced as the simulated annealing temperature is decreased. The method for reducing the temperature is called the quenching schedule; the simplest method is one that decreases the temperature by a constant amount per simulated annealing iteration. A successful run generates a number of possible structures of different energies. Structures with energies no more than 0.02 hartrees above the lowest energy of the set are selected for a final optimization. As an example, Table 2 shows typical parameters for the calculation of Li_q ($q=5-7$) clusters.

Notice that the modification of the acceptance criteria in principle allows for a relatively exhaustive sampling of potential energy search that could lead to the generation of the most physically relevant structures. Fig. 4 shows the results of a typical simulated annealing optimization of the Li_7^+ cluster. Most of the observed structures are sampled early on in the simulated annealing procedure as a result of producing Markov chains generated at high temperatures, which allows the algorithm to “jump” over potential energy barriers with relative ease. As the annealing temperature is reduced, the number of accepted structures tends toward the minimum energy set of structures, reducing the scope of the sampling.

In Ref. [33] the procedure described above was applied to $\text{Li}_q^{-0,+}$ ($q=5-7$) clusters, and some new structures were reported. Most of the isomers agree very well with previous work [34–36]. The method was also applied to the more complex binary Li_5Na cluster where six isomers were found [33].

The Big Bang method

The “big bang” method [37, 38] is the simplest of the three methodologies discussed in this chapter, and the only one specifically designed for geometry optimization of clusters. It starts with a relatively large population of geometrical structures that is chosen randomly and enclosed in a

very small volume. Then, using standard geometry optimization procedures, one proceeds to relax the structures by following the force (negative gradient). Since at the beginning all the atoms are very close each other, the repulsive forces among them are very large and consequently they tend to “explode,” landing in distant parts of the hypersurface. By starting with a large population, one can be certain to explore a large portion of the hypersurface. By optimizing individual structures, the procedure produces different local minima including, hopefully, the global minima. The method is very simple to implement, but curiously has not been adopted by the chemistry community. In the implementation developed in Ref. [39], $1000N$ random structures were generated, where N is the number of atoms in the cluster. These were confined to a volume proportional to the covalent radius of the atom and the structures were optimized using the semiempirical MSINDO method [26]. The optimized structures were then optimized at a higher level of theory.

In this way, more than 70 different isomers of Li_n ($n=3-20$) have been found [39]. In Table 3, the symmetry of the reported structures is compared with other work. More than 50 new structures are reported. The big bang methodology has been also applied to sodium and potassium clusters [39].

The three methodologies discussed in this section are all based in the use of stochastic techniques. In each of the methods there is no guarantee of reaching the global minimum, and one should perform the minimization various times with different starting structures to be sure that a consistent set of minimum-energy isomers is obtained. In general, the choice of which method to use is more a matter of convenience, especially with respect to the computational facilities, than a formal decision based on theoretical grounds. In the cases discussed here, a detailed comparison for the small members of the series indicates that the three methodologies discussed above are able to locate the lowest energy isomers and the differences lie more in the efficiency of the implementation rather than in some formal advantage of the method.

4. Analysis of the chemical bonding and reactivity of atomic clusters

Most atomic clusters possess very labile bonds that do not follow the ordinary chemical rules describing the bonding and geometry of ordinary molecules such as hydrocarbons. For instance, they can present a lower or higher coordination than the one dictated by the number of valence electrons: the simple octet rule is almost never followed. Therefore, the number of possible isomers increases dramatically (usually exponentially) with the number of atoms and chemical intuition does not help in predicting the most stable isomer. This presents two issues to the theoretical calculations. First, how can one find the most stable isomers (global minima) when most optimization techniques do not guarantee that a global minimum will be found? Second, how can one understand the bonding between the atoms in a cluster? Once the geometric parameters of the lowest energy isomers of a given cluster are known, the task is to try to understand the way the atoms are bonded to one another. This knowledge permits the prediction of new geometries and prediction of the class of reactivity the cluster can undergo. Unfortunately, this is not an easy task, and until recently there has been no simple model for understanding bonding in atomic clusters. Generally, the Lewis electron pair model does not work and one has atomic clusters that are either electron deficient or hypervalent. Often it is difficult to predict the multiplicity of the ground state. In addition, the widely popular Mulliken population analysis tends to predict the incorrect electron charge distribution in atom pairs, and even the more robust natural bond order (NBO) method can fail in cases of extremely delocalized bonds that are common in atomic clusters. One of the most useful theoretical tools for analyzing bonding in atomic clusters is the Electron Localization Function (ELF).

The ELF was originally proposed by Becke and Edgecombe [40] and is defined as

$$ELF(\vec{r}) = \left[1 + \left(\frac{T[\rho(\vec{r})]}{T_0[\rho(\vec{r})]} \right)^2 \right]^{-1} \quad (2)$$

where $T[\rho(\vec{r})] = T_s[\rho(\vec{r})] - T_w[\rho(\vec{r})]$ is the kinetic energy density difference between the kinetic energy density of the non-interacting system $T_s[\rho(\vec{r})]$ with density $\rho(\vec{r})$, and the von

Weizsacker kinetic energy density, $T_w[\rho(\vec{r})]$. In addition, $T_0[\rho(\vec{r})]$ indicates the kinetic energy density of the noninteracting electron gas. The important quantity in equation 2 is the term $T[\rho(\vec{r})]$ that can be interpreted [41] as the excess kinetic energy density due to the Pauli exclusion principle. Simple analysis of Equation [2] indicates that the function $ELF(\vec{r})$ varies between 0 and 1. The interpretation of the function is that the region of the space where the ELF has a value close to 1 corresponds to the regions where it is most probable to find a localized electron pair; regions with a low value of the ELF (≈ 0.5) correspond to regions where the electrons are delocalized. Hence, the interpretation of ELF isosurfaces allows us to understand bonding in clusters. For a more detailed description of the ELF, see Ref. [40].

As an example of the utility of the ELF, we show in panel (a) of Fig. 5 the position of the atoms of one of the isomers of the cluster of Li_6 . The lines in this figure serve to guide the eyes and they do not represent electrons in the sense of the Lewis structures. The cluster has only six valence electrons and the question is: how are the six atoms are bonded to one another with only six electrons? The ELF isosurface depicted in panel (b) gives a clear answer. There are three equivalent regions where the electrons are most probably localized forming *two electron-three center* bonds.

The applications of the ELF have been very successful in all fields of chemistry and physics [41, 42]. Recently, the ELF has been used to understand and quantify the concept of aromaticity in metallic clusters [43, 44]. Unfortunately, its use for clusters formed by heavy atoms is not free of complications and the issue remains open to interpretation.

Once the geometry of a given cluster and the types of bonds it forms are understood, the next step is to predict how the cluster will react in the presence of a given atom or molecule. There have been various studies of the reactivity of clusters. For example, the bonding of a hydrogen atom to a lithium cluster has been analyzed using the ELF [45]. The reactivity of a particular silicon cluster, Si_4 , with a Ga atom has been studied using reactivity indices defined within density

functional theory [46, 47]. The topology of the frontier orbitals was used in Refs. [48, 49] to propose simple rules to predict the binding sites in Au and Ag clusters. The bonding and reactivity between H and the Al₁₃ cluster has been studied using the Fukui function [50]. It is very important to understand how a cluster forms and how it will react in presence of other species. Once the most stable isomers of an atomic cluster are found, it is necessary to calculate as accurately as possible properties that may be compared to experimental measurements. Only in cases where the theoretical calculations agree with the results of the experimental measurements can one have confidence in the prediction of the most stable isomer. From the considerations above, it is clear that the theoretical study of atomic clusters is a rather cumbersome task involving a variety of theoretical methodologies.

In Ref. [51], a recently proposed version of the local Fukui function has been applied to the study of the reactivity of silicon clusters in presence of a hydrogen atom. The Fukui function has been defined by Parr and Yang [52] as

$$f(\vec{r}) = \left(\frac{\delta\mu}{\delta v(\vec{r})} \right)_N \quad (3)$$

where μ is the chemical potential, $v(\vec{r})$ is the external potential and the derivative is taken at a constant number of electrons N . Using the frozen orbital approximation, the derivative in Equation 3 can be evaluated as the square of the frontier molecular orbital – the square of the HOMO if the derivative is approximated from the left and the square of the LUMO if the derivative is approximated from the right. The distinction is due to the known discontinuity of the density as N passes through an integer value [46]. Hence, the Fukui function can be approximated as

$$f^\pm(\vec{r}) = |\phi(\vec{r})|^2 \quad (4)$$

where $\phi(\vec{r})$ is the frontier molecular orbital, and the sign \pm means the HOMO or LUMO, respectively. A condensed form of this function using the integration of the proper Fukui function over its own basins has been proposed as a better alternative than using population analysis [53]. In Ref. [51] this condensed form has been used to study the reaction of hydrogen atom with

silicon clusters. The theoretical predictions of the sites of most probable attack have been confirmed by computational simulations where the genetic algorithm has been used to find the most stable clusters of Si_nH . Given that the chemical potential, defined as the negative of the absolute electronegativity, has a value of -7.25 eV for the hydrogen atom and is in the range of -4.5 to -5.0 eV for silicon clusters, it is expected that the silicon clusters will donate charge to the hydrogen atom and therefore the Fukui function should be calculated with the square of the HOMO.

On the left column in Figure 6 the geometrical structures of the clusters of Si_3 , Si_4 , Si_5 and Si_7 have been depicted while in the right column the respective Fukui function isosurfaces and their condensed values over the basins are also shown. They are calculated as the integral of the Fukui function over the respective volume. Larger numbers indicate more reactive regions. Therefore, one expects that a hydrogen atom would bind the cluster in the zone where the condensed Fukui function has the largest value. In fact, in Ref. [51] it was found that the predicted cluster was always one of the most stable ones. Exceptions occur when the hydrogenated cluster drastically alters the Si_n skeleton of the Si_nH cluster with respect to the initial silicon cluster. A similar methodology has also been used to explain and predict the reactivity of copper clusters with molecular oxygen [54].

5. Unique Physical Properties of Clusters and Their Relation to the Corresponding Surface and Bulk Properties

As mentioned above, atomic clusters show many distinct properties from those of isolated atoms or bulk solids that can be very useful in practical applications. At the same time, there is the possibility to analyze known phenomena from a new perspective. For example, the discovery of giant plasmon resonances in metal clusters [55, 56] and in fullerenes [57, 58] allowed scientists to study the transition from the classical Mie picture of plasmon oscillations to the quantum limit or to detect cluster deformations by the value of the splitting of plasmon resonance frequencies [3, and references therein]. In this section we briefly discuss another very interesting phenomenon: the onset of magnetism in bare and ligand-coated clusters of gold, a typical diamagnetic metal. We emphasize the usefulness of clusters as 'transition structures' that facilitate a better understanding of magnetism in molecular and extended systems (surfaces or solids).

One of the first observations of magnetism in gold was reported by Zhang and Sham [59] in their X-ray spectroscopic study of alkane-thiolated nanoclusters. Later, Crespo et al. [60] used X-ray absorption near-edge structure (XANES) measurements to show the appearance of ferromagnetism accompanied by room-temperature hysteresis in thiol-capped Au nanoparticles with a diameter of 1.4 nm. This rather surprising finding led to the proposal that the strong chemisorption of ligands into relatively small nanoparticles of bulk-diamagnetic materials could induce permanent magnetism as a result of electronic structure effects involving interactions between the *sp*-orbitals of the adsorbate and the *5d*-orbitals of the Au atoms lying on the surface of the nanoparticle. This mechanism was later questioned by the results reported by Hori and collaborators [61] based on superconducting quantum interference device magnetometer (SQUID) measurements of a series of Au nanoparticles protected by strongly interacting thiols such as dodecane thiol (DT) and weakly coupled ligands such as polyacrylonitrile (PAN), polyallyl amine hydrochloride (PAAHC), and polyvinyl pyrrolidone (PVP). In this study the authors

found that the strong chemisorptive interaction between the sulfur atom in DT and the Au atoms on the surface of the nanoparticle induced a spin singlet state that significantly decreased the magnetization of the system (although it did not quench it completely) when compared to the corresponding magnetization measured in Au nanoparticles capped with weakly coupled ligands such as PAN, PAAHC and PVP. In the same study, Hori and collaborators report that the measured magnetization is strongly size dependent, increasing with particle diameter at the smaller nanoparticle sizes, peaking at approximately 3 nm for Au-thiol nanoparticles, and subsequently decreasing with increasing nanoparticle size, keeping with the fact that as the Au nanoparticle size increases, its configuration approaches that of the bulk lattice [61]. Additionally, a closely related phenomenon has been observed in gold surfaces: the occurrence of magnetism when organic molecules are self-assembled as monolayers on a surface [62]. The observed magnetism has been attributed to charge transfer between the organic layer and the metal substrate [62].

These effects are somehow intriguing given that gold is a diamagnetic metal, but perhaps not totally unexpected. Close examination of Stoner's model [63] suggests that the emergence of "unexpected" magnetic ordering in transition metal clusters in confined spaces at the nanoscale is possible. In this model, the paramagnetic susceptibility χ is determined by the density of d states at the Fermi level $N(E_F)$ and the exchange function J ,

$$\chi = \frac{\mu_0 \mu_B^2 N(E_F)}{(1 - JN(E_F))} \quad (5)$$

where μ_0 is the permeability of free space and μ_B is the Bohr magneton (9.27×10^{-24} J/T). The spatial confinement produces a narrower d -band, and eventually the center of the band is shifted closer to the Fermi level. For $JN(E_F) > 1$, the term $1 - JN(E_F)$ in Eq. 5 becomes negative, consequently generating ferromagnetic instability, and thus magnetic order.

Several previous experimental studies have shown that the onset of magnetism at the nanoscale occurs in a complicated way with clusters frequently having unusual magnetic properties not

clearly related to the strength and orientation of the metal bulk magnetization. Stern-Gerlach molecular-beam deflection experiments [64–69] with bare clusters of transition metals show either high-field deflection indicative of superparamagnetism or symmetric broadening indicative of locked moment behavior. These clusters exhibit susceptibilities significantly larger in magnitude than those expected based on the extrapolation of the susceptibility of the bulk solids. It is worth mentioning also that molecules comprising a large number of coupled paramagnetic centers capped by ligands (e.g. Mn_{12} and Fe_8 families) are known to show unambiguous evidence of quantum size effects in magnets [70].

Magnetism in bare (uncapped) gold nanoclusters has been explored in our group [71] from a spin-dependent density-functional theory (DFT) perspective with scalar relativistic effects included via the use of pseudo-potentials. In this study, three different DFT exchange-correlation energy functionals were used: the Perdew, Burke, and Ernzerhof [72] generalized gradient approximation (PBE), and the hybrid functionals B3LYP [73] and PBE1PBE [74]. In addition, two different basis sets were chosen: a single valence plus polarization with the Stuttgart [75] effective core potential (SVP/STUTT) basis (27 basis functions comprised of 55 primitive gaussians), and the LANL2DZ [76] basis set developed by the Los Alamos group (24 basis functions comprised of 44 primitive gaussians) with its respective effective core potential. The calculated electronic structures of gold nanoclusters of different sizes (Au_n , with $n = 2, 14, 28, 38, 56$, and 68) reveal that they exhibit (with the exception of Au_2) a core-shell geometric arrangement of Au atoms and that permanent size-dependent spin-polarization appears without geometry relaxation for bare clusters even though bulk gold is diamagnetic [71]. The spin-polarized ground states for clusters are favorable due to the hybridization of the s and d orbitals, and bare octahedral clusters are expected to be magnetic for cluster sizes of approximately 38 atoms and larger. Much larger clusters will be diamagnetic when the surface-to volume ratio is small and the core diamagnetism prevails.

Making use of these findings, we developed a spin-spin Ising interaction model [77] that explains the origin of the size dependency of magnetization in Au clusters. This model combines the bulk diamagnetic response of the core with surface (shell) ferromagnetism behavior (as suggested by the results in ref. [71]). In this model, the Maximum Entropy formalism is used in order to obtain an average temperature-dependent magnetization of bare Au nanoparticles within a mean-field theory. Accordingly, the total Hamiltonian H_T can be partitioned into a core H_c and a surface H_s contribution:

$$\boxed{\text{Diagram showing a red 'X' mark}} \quad (6)$$

with

$$H_c = -\sum_{i < j}^{N_c} \sum_j^{N_c} J_{ij}^c \cdot \vec{S}_i \cdot \vec{S}_j - \frac{1}{2} \sum_i^{N_s} \sum_j^{N_c} J_{ij}^{sc} \cdot \vec{S}_i \cdot \vec{S}_j - \sum_i^{N_c} k_c \cdot S_{z_i}^2 \quad (7)$$

and

$$H_s = -\sum_{i < j}^{N_s} \sum_j^{N_s} J_{ij}^s \cdot \vec{S}_i \cdot \vec{S}_j - \frac{1}{2} \sum_i^{N_s} \sum_j^{N_c} J_{ij}^{sc} \cdot \vec{S}_i \cdot \vec{S}_j - \sum_i^{N_s} k_s \cdot |\hat{n}_r \cdot \vec{S}_i|^2 \quad (8)$$

In equations (7) and (8), N_c and N_s indicate the number of core and surface Au atoms, respectively, such that the total number of atoms $N = N_c + N_s$. The interaction terms are partitioned into $N_s(N_s - 1)$ surface atom interactions, $N_s N_c$ core atom interactions with the surface atoms and $N_c(N_c - 1)$ core atoms interactions with coupling functions J^s , J^{cs} , J^{sc} and J^c , respectively (with $J_{ij}^x > 0$ for ferromagnetic interactions). In addition, the last terms in Equations (7) and (8) describe the anisotropy term spin with the Hamiltonian assumed to be aligned along the radial direction \hat{n}_r , with k_c and k_s being the anisotropy constants for the core and surface spins respectively. After some algebraic manipulations making use of the maximum spin entropy approach (see ref. [77] for details) the following expression for the total magnetic moment per atom μ_t is obtained

$$\mu_t = \frac{N_s}{N_t} \left(1 - v \cdot J^s \cdot N_s (N_t - N_s) \right)^{\frac{1}{3}} \quad (9)$$

where the surface magnetic moment μ_s can be obtained self-consistently from the following expressions

$$\mu_s = \tanh\left(\frac{1}{k_B T} \left[\frac{1}{g} J^s \cdot N_s \cdot \mu_s + g \cdot h_z \right]\right) \quad (10)$$

$$\mu_s = \tanh(\xi); \quad (11)$$

$$\xi = \frac{1}{k_B T} \left(\frac{1}{g} J^s \cdot N_s \cdot \mu_s + g \cdot h_z \right)$$

In expressions [9] – [11], J^s indicates the average surface exchange, g is related to the gyromagnetic constant, h_z is the effective field in the preferred z direction, and the constant ν is given by

$$\nu = \frac{3^{1/3} e^2}{12 \pi^{4/3} m_e c^2} \tilde{\lambda} \quad (12)$$

with e and m_e indicating the charge and mass of an electron, c the speed of light and $\tilde{\lambda}$ is a phenomenological constant. Figure 7 depicts a plot of the magnetic moment per atom as a function of the particle size for a typical gold nanoparticle. The results show how this simple Ising model reproduces qualitatively the size dependence behavior observed experimentally by Hori and collaborators [61].

We have also performed studies aimed at understanding the origins of magnetic behavior in gold upon chemisorption as well as the effect of different ligands on the magnetic moment. Using a simple quantum chemical model based on Finite Perturbation Theory (FPT) combined with Density Functional Theory calculations on a Au cluster with a two-layer slab of 13 atoms (9 in the first layer and 4 in the second layer), Gonzalez et al. [78] were able to suggest ideas regarding the electronic structure origin of the observed magnetism in Au cluster-ligand systems with different chemical linkers, and provided a theoretical basis to rationalize the experimental observation indicating that magnetism can be induced in gold as a result of the chemisorption of S-linked ligands, whereas weakly coupled linkers such as N do not affect the diamagnetic

behavior of Au surfaces. In particular, it was shown that for some linkers such as sulfur, a spin symmetry breaking occurs that lowers the energy and leads to preferential spin density localization on the gold atoms neighboring the chemisorption site. These preliminary results seem to be in agreement with the conjecture proposed by Crespo et al. [60] that the interaction between S and Au orbitals is responsible for the onset of magnetism in thiol-capped gold nanoclusters. However, in order to confirm this proposal, similar calculations using the FPT model should be performed on larger clusters with core-shell structures typical of Au nanoparticles.

Our group has also performed electronic structure calculations on larger clusters (Au_{23} and Au_{55}) in order to reproduce and study the magnetic behavior of high electric dipole moment thiopolypeptide R-helix linkers, (consisting of 8 L-glycine units) chemisorbed on the (111) Au surfaces [79]. The wave function broken symmetry method (BS-UDFT) was used for this purpose [80]. The results of this study indicate a strong correlation between the magnetic behavior of the adsorbate-cluster system and the orientation of the electric dipole of the R-helix and charge-transfer at the molecule-metal interface. Upon chemisorption, dipole moments may be quenched or enhanced with respect to the gas phase value. The results of this study indicate that the strongest reduction in dipole moment accompanied with net charge-transfer from the Au surface leads to a very stable magnetic state. Additionally, it was found that the magnetic properties of these systems are strongly dependent on the size and geometrical structure of the Au cluster under consideration.

In addition to the cluster calculations, we have also studied the effect of benzenethiol chemisorption on the magnetic properties of gold films [81] via DFT calculations on extended systems. Gold films have been modeled by constructing slabs from the Au (111) lattice, containing from 1 to 4 layers, with 3x3 atoms in each layer. Spin-polarized DFT calculations have been performed using the SIESTA package [82]. This code allows electronic structure calculations of extended systems using pseudopotentials with periodic boundary conditions, where numerical atomic orbitals are used as basis sets to solve the single-particle Kohn-Sham

equations. Our calculations were performed within the PBE generalized gradient approximation of density-functional theory, using norm-conserving Troullier-Martins pseudopotentials [83] as implemented in the SIESTA software. We use a double-zeta basis set with polarization orbitals on all the atoms [84]. The real-space mesh used for the calculation of the charge density and evaluation of real-space integrals is defined by a ‘mesh cut-off’ parameter, defining the maximum energy of plane waves that can be represented on the mesh without aliasing. This parameter was set to 350 Ry for all calculations. The supercell dimensions were kept fixed for all calculations ($a=b=8.65$ Å, $c=30$ Å).

Figure 8 depicts a plot of the variation of the magnetic moment with the number of layers in the gold films. As observed in this plot, the total magnetic moment decays exponentially as the number of layers increases, approaching a value of zero for 4 layers. This magnetic behavior in has recently been observed experimentally in gold films [4]. In the case of the 4-layer supercell capped with benzenethiol, our calculations show an onset of a finite magnetic moment of approximately $0.025 \mu_B$ per absorbed molecule. The fact that this value is smaller than the experimental one (on the order of $10 \mu_B$; see ref. [62] for details), is not surprising given the limitation of the size of unit cell used in our calculations and also due to the fact that our calculations do not explicitly include important spin-orbit coupling effects. Finally, population analysis of this system suggests that the majority of “spin up” electrons are predominantly localized on the surface and shared equally among the atoms. Small “diamagnetic” contributions on the bulk atoms are also found.

Overall, our theoretical calculations show that chemisorbed thiolates on gold surfaces induce magnetism, basically due to a local Pauli repulsion between the sulfur and the gold atoms in the neighborhood of the chemisorption site. However, the results also show that bare Au clusters have the an intrinsic tendency to exhibit magnetic behavior suggesting that it is quite possible that the origin of chemisorption-induced magnetism on Au surfaces might indeed be different from a simple spin symmetry breaking on the surface atoms in Au clusters with core-shell structures. It

should be noted that despite the interesting results of this study, other aspects of this problem remain unclear, including the origin of the very small hysteresis and the high anisotropy of this magnetism. In order to answer these questions, more elaborate and theoretical models should be developed.

Although not an exhaustive review, this Chapter briefly illustrates the potential benefits of applying theory and quantum chemistry calculations in understanding diverse intricate physical and chemical phenomena related to metallic clusters. More than a predictive tool replacing experimental measurements, these techniques should be considered as an important complement to measurement sciences and metrology aimed at helping with the interpretation of experimental results and the proposal of new measurement campaigns.

Acknowledgment

PF thanks Fondecyt, grant 1080184, Chile, and the NIST foreign visitor program for financial support.

References

1. G. P. Wiederrecht, Editor, *Handbook of Nanofabrication*, Amsterdam-Boston, Elsevier, 2010.
2. F. Papanelopoulou, *Between Physics and Chemistry: Early-Low-Temperature Research, 1877-1908*, 6th International Conference on the History of Chemistry, Leuven (Belgium), 2007.
3. J.P. Connerade, A.V. Solov'yov and W. Greiner, *Europhysicsnews* 33 (6), 200-202, 2002.
4. S. Reich, G. Leitus, and Y. Feldman, *Applied Physics Letters* 88, 222502, 2006.
5. D. J. Sellmyer, M. Yu, R. A. Thomas, Y. Liu, and R. D. Kirby, Nanoscale design of films for extremely high density magnetic recording, *Phys. Low-Dimensional Structures*, vol. 1/2, 1998. Proceedings of the Ninth Joint MMM/Intermag Conference, *J. Appl. Phys.*, pt. 2, vol. 95, 2004.
6. W. Knight, K. Clemenger, W. A. de Heer, W. Saunders, M. Chou and M. Cohen, *Phys. Rev. Lett.* 52, () 2141, 1984.
7. W. Ekardt, *Phys. Rev. Lett.* 52, 1925, 1984.
8. M. Brack, *Rev. Mod. Phys.* 65, 677, 1993.
9. W. de Heer, *Rev. Mod. Phys.* 65, 612, 1993
10. P. Hohenberg and W. Kohn, *Phys. Rev.* 136, B864, 1964.
11. W. Kohn and L. Sham, *Phys. Rev.* 140, A1133, 1965.
12. Y. Simón-Manso Doctoral Thesis, Pontifical Catholic University of Chile, 1998.
13. W.A. Harrison, *Electronic Structure and the Properties of Solids: The Physics of the Chemical Bond*, Dover Publications, Inc., New York, 1989.
14. Z. Yu and J. Almlof, *J. Phys. Chem.* 95, 9167-9169, 1991.
15. A. N. Andriotis, N. N. Lathiotakis and M. Menon *Europhys. Lett.*, 36 (1), 37-42, 1996.
16. A. D. Becke, *Phys. Rev.*, A38, 3098, 1988.
17. J. P. Perdew, *Phys. Rev.*, B33, 8822, 1986
18. W. J. Hehre, R. Ditchfield and J. A. Pople *J. Chem. Phys.* 56, 2257, 1972.
19. D. R. Lide, Editor, *CRC Handbook of Chemistry and Physics, 75th Edition* CRC Press, Boca Raton, FL., 1994.

20. P. Fuentealba Y. Simón-Manso *Chemical Physics Letters*, 314, 1, 108-113, 1999.
21. D. Marx, in *Computational Nanoscience: Do it yourself*, pg. 195 NIC Series vol.31, 2006.
22. V. Bazterra, M. Caputo, M. Ferraro and P. Fuentealba, *J. Chem. Phys.* 117, 11158, 2002.
23. M. Iwamatsu, *J. Chem. Phys.* 112, 10 976, 2000.
24. C. Roberts, R. L. Johnston, and N. T. Wilson, *Theor. Chem. Acc.* 104, 123, 2000.
25. V. E. Bazterra, M. B. Ferraro, and J. C. Facelli, *J. Chem. Phys.* 116, 5984, 2002.
26. T. Bredow, G. Geudtner and K. Jug, *J. Comput. Chem.* 22, 861, 2001.
27. G. Igell-Mann, H. Stoll and H. Preuss, *Mol. Phys.* 65, 1321, 1988.
28. A. Sadlej *Collect. Czech Chem. Commun.* 53, 1995, 1998.
29. O. Oña, V. Bazterra, M. Caputo, J. Facelli, P. Fuentealba and M. Ferraro *Phys. Rev. A* 73, 053203, 2006.
30. Q. Sun and Y. Kawozoe *Phys. Rev. Lett.* 90, 135503, 2003.
31. N. Metropolis, N. Rosenbluth, M. Rosenbluth and E. Teller *J. Chem. Phys.* 21, 1087, 1953.
32. E. Aarts and H. Landhooven, *Simulating Annealing, Theory and Application*, Springer, New York, 1987.
33. J. Perez, E. Florez, C. Hadad, P. Fuentealba and A. Restrepo *J. Phys. Chem A* 112, 5749, 2008.
34. B. Temelso and D. Sherrill *J. Chem. Phys.* 122, 064315, 2005.
35. A. Alexandrova, A. Boldyrev, *J. Chem. Theory Comput.* 1, 566, 2005.
36. E. Florez and P. Fuentealba *Int. Journal of Quantum Chem.* 109, 1080, 2009.
37. R. H. Leary, *J. Global Optim.* 11, 35-53, 1997.
38. K. A. Jackson, M. Horoi, I. Chaudhuri, T. Frauenheim, A. A. Shvartsburg, *Phys. Rev. Lett.* 93, 013401, 2004.
39. J. Centeno and P. Fuentealba to be published. *Int. Journal Quantum Chem.* Accepted for publication, 2010.
40. A. Becke and K. Edgecombe *J. Chem. Phys.* 92, 5397, 1990.
41. A. Savin, O. Jepsen, J. Flad, O. Anderson, H. Preuss and H. von Schnering *Angewandte Chemie* 31, 187, 1992.

42. P. Fuentealba, E. Chamorro and J. C. Santos, pg. 57, in *Theoretical Aspects of Chemical Reactivity*, Ed. by A. Toro, Elsevier, 2007.
43. B. Silvi and A. Savin *Nature* 371, 683, 1994.
44. B. Silvi, E. Fourre and M. Alikhani *Monatshefte fuer Chemie* 136, 855, 2005.
45. J. C. Santos, W. Tiznado, R. Contreras and P. Fuentealba, *J. Chem. Phys.* 120, 1670, 2004.
46. R. G. Parr and W. Yang, *Density Functional Theory of Atoms and Molecules*, Oxford Press, 1990.
47. J. C. Santos, J. Andres, A. Aizman and P. Fuentealba *J. Chem. Theory Comput.* 1, 83, 2005.
48. P. Fuentealba and A. Savin *J. Phys. Chem. A* 105, 11531, 2001.
49. M. Galvan, A. dal Pino, J. Joannopoulos *Phys. Rev. Lett.* 70, 21, 1993.
50. S. Crhétien. M. Gordon and H. Metiu *J. Chem. Phys.* 121, 3756, 2004.
51. S. Crhétien. M. Gordon and H. Metiu *J. Chem. Phys.* 121, 9931, 2004.
52. R. Parr and W. Yang *J. Am. Chem. Soc.* 105, 4049, 1984.
53. W. Tiznado, O. Oña, V. Bazterra, M. Caputo, J. Facelli, M. Ferraro and P. Fuentealba *J. Chem. Phys.* 123, 214302, 2005.
54. E. Florez, F. Mondragon and P. Fuentealba *J. Phys. Chem. B* 110, 13793, 2006.
55. C. Bréchnignac, Ph. Cahuzac, F. Carlier and J. Leygnier *Chem. Phys. Lett.* 164, 433, 1989.
56. K. Selby, V. Kresin, J. Masui, M. Vollmer, W. A. de Heer, A. Scheidemann and Knight W D *Phys. Rev. B* 43, 4565, 1991.
57. G. F. Bertsch, A. Bulgac, D. Tomanek, and Y. Wang *Phys. Rev. Lett.*, 67, 2690, 1991.
58. G. Barton and C. Eberlein *J. Chem. Phys.* 95, 1512, 1991.
59. P. Zhang; T.K. Sham *Phys. Rev. Lett.* 90, 245502, 2003.
60. P. Crespo, R. Litrán, T. C. Rojas, M. Multigner, J. M. de la Fuente, J. C. Sánchez-López, M. A. García, A. Hernando S. Penadés,; A. Fernández, *Phys. Rev. Lett.* 93, 087204, 2004.
61. H. Hori, Y. Yamamoto, T. Iwamoto, T. Miura, T. Teranishi, M. Miyake *Phys. Rev. B* 69, 174411, 2004.
62. I. Carmeli, G. Leitun, R. Naaman, S. Reich, and Z. Vager, *J. Chem. Phys.* 118, 10 372, 2003.
63. E.C. Stoner *Proc. R. Soc.* 154, 656-78, 1936; and *Proc. R. Soc.* 169, 339-71, 1939.

64. M. B. Knickelbein *Phys. Rev. B* 71, 184442, 2005.
65. J. Cox, J. G. Louderback, S. E. Apsel, and L. A. Bloomfield, *Phys. Rev. B* 49, 12295, 1994.
66. L. A. Bloomfield, J. Deng, H. Zhang, and J. W. Emmert, in *Proc., International Symposium on Cluster and Nanostructure Interfaces*, edited by P. Jena, S. N. Khanna, and B. K. Rao World Publishers, Singapore, 2000.
67. M. B. Knickelbein, *Phys. Rev. Lett.* 86, 5255, 2001.
68. M. B. Knickelbein, *Phys. Rev. B* 70, 014424, 2004.
69. J. Cox, J. G. Louderback, and L. A. Bloomfield, *Phys. Rev. Lett.* 71, 923, 1993.
70. D. Gatteschi, R. Sessoli *Angew. Chem. Int. Ed.* 42, 268-297, 2003.
71. R.J. Magyar, V. Mujica, M. Marquez, and C. Gonzalez *Phys. Rev. B* 75, 144421, 2007.
72. Perdew, J. P.; Burke, K.; Ernzerhof, M. *Phys. Rev. Lett.* 77, 3865, 1996.
73. A.D. Becke, *J. Chem. Phys.*, 98, 5648, 1993.
74. J. P. Perdew, K. Burke, M. Ernzerhof, *Phys. Rev. Lett.* 78, 1396, 1997.
75. A. Schaefer, C. Huber, R. Ahlrichs *J. Chem. Phys.* 100, 5829, 1994.
76. W.R. Wadt, P.J. Hay *J. Chem. Phys.* 82, 284, 1985.
77. F. Michael, C. Gonzalez, V. Mujica, M. Marquez, M. Ratner, *Phys. Rev. B* 76, 224409, 2007.
78. C. Gonzalez, Y. Simón-Manso, M. Marquez, M. Ratner and V. Mujica *J. Phys. Chem. B* 110, 687-691, 2006.
79. L. Puerta, H. J. Franco, J. Murgich, C. Gonzalez, Y. Simón-Manso, and V. Mujica *J. Phys. Chem. A* 112, 9771–9783, 2008.
80. J. Gräfenstein, E. Kraka,; M. Filatov, and D. Cremer *Mol. Phys.*, 99, 1899-1940, 2001 and D. Cremer *Int. J. Mol. Sci.* 3, 360-394, 2002.
81. Y. Simón-Manso, M. Marquez, Mujica V. and C. Gonzalez Altria-INEST meeting, Williamsburg, VA, May 17-19, 2005.
82. E. Artacho, D. Sanchez-Portal, P. Ordejon, A. Garcia and J.M. Soler *Linear-scaling ab-initio calculations for large and complex systems, Physica Status Solidi (b)*, 215, 809, 1999.
83. N. Troullier and J.L. Martins *Efficient pseudopotentials for plane-wave calculations Phys. Rev. B* 43, 1993, 1991.

84. O. F. Sankey, D. Niklewski, *Phys. Rev. B* **40**, 3979, 1989.

Table 1. Energy of the **HOMO**, binding energy per atom, dipole polarizability and energy **gap** for the low-lying isomers of Si₉.

Cluster	Symm	ε_H (a.u.)	E_B/atom (eV/atom)	α (Å/atom)	Gap(eV)
I	C _s	-0.223	-3.055	4.73	2.77
II	C ₂	-0.212	-2.994	4.91	2.07
III	C _{2v}	-0.219	-2.988	4.80	2.77
V	C ₂	-0.210	-2.945	4.79	1.99
VI	C _s	-0.207	-2.931	4.90	2.37
VII	C _{2v}	-0.205	-2.828	5.27	2.37
VIII	C _{2v}	-0.195	-2.788	5.31	1.99

Table 2. Typical Simulated Annealing parameters.

Parameter	Li ₅	Li ₆	Li ₇
generated structures	49	111	33
with $\Delta E < 0$	14	10	8
with $\Phi(\Delta E) < P(\Delta E)$	35	101	25
finally located minima	2	3	2

Table 3. Isomers of lithium clusters

Li_n	This work (Big-Bang)	Jones ²⁵	Gardet ²⁶
3	$\text{C}_{2v}^{\text{P}}, \text{D}_{\infty h}^{\text{L}}$	$\text{C}_{2v}^{\text{P}}, \text{D}_{\infty h}^{\text{L}}$	C_{2v}^{P}
4	D_{2h}^{P}	D_{2h}^{P}	D_{2h}^{P}
5	$\text{C}_{2v}, \text{C}_{2v}^{\text{P}}$	$\text{C}_{2v}, \text{C}_{2v}^{\text{P}}$	$\text{C}_{2v}, \text{C}_{2v}^{\text{P}}$
6	$\text{D}_{4h}, \text{C}_{5v}, \text{D}_{3h}, (\text{D}_{2d})$	$\text{D}_{4h}, \text{C}_{5v}, \text{D}_{3h}$	$\text{D}_{4h}, \text{C}_{2v}, \text{D}_{3h}$
7	$\text{D}_{5h}, \text{C}_{3v}, (\text{C}_s)$	$\text{D}_{5h}, \text{C}_{3v}$	D_{5h}
8	$\text{T}_d, (\text{C}_{3v}), (\text{C}_s)$	$\text{D}_{5h}, \text{T}_d, \text{C}_{2v}$	$\text{T}_d, \text{C}_{2v}, \text{C}_s$
9	$\text{C}_{4v}, \text{C}_{2v}, \text{C}_s$	$\text{C}_s, \text{C}_{4v}$	$\text{C}_{2v}, \text{C}_s$
10	$(\text{D}_{2d}), (\text{C}_s), (\text{C}_{4v}), (\text{T}_d)$	$\text{C}_1, \text{C}_{2v}$	$\text{C}_1, \text{C}_{2v}$
11	$\text{C}_2, (\text{C}_{2v}), (\text{C}_2), (\text{C}_s)$		C_2
12	$\text{C}_s, (\text{C}_s), (\text{C}_{2v})$		C_s
13	$(\text{C}_s), (\text{C}_s), (\text{C}_2), (\text{C}_1), (\text{C}_1), (\text{C}_{3v})$		C_s, C_1
14	$(\text{C}_2), (\text{C}_s), (\text{C}_{3v}), (\text{C}_s), (\text{C}_1), (\text{C}_1)$		
15	$(\text{C}_{4v}), (\text{C}_1), (\text{C}_2), (\text{C}_s), (\text{C}_1), (\text{C}_s), (\text{C}_s)$		
16	$(\text{C}_s), (\text{C}_1), (\text{C}_1), (\text{C}_1), (\text{C}_1)$		
17	$(\text{C}_1), (\text{C}_s), (\text{C}_1)$		
18	$(\text{C}_s), (\text{C}_1), \text{C}_{5v}, (\text{C}_1), (\text{C}_1), (\text{C}_1), (\text{C}_s), (\text{C}_1), (\text{C}_{4v})$		$\text{C}_{5v}, \text{D}_{5h}, \text{D}_{3h}, \text{C}_1$
19	$(\text{C}_{2v}), (\text{C}_s), (\text{C}_1), (\text{C}_1)$		D_{5h}
20	$\text{C}_s, (\text{C}_1), \text{C}_{2v}, (\text{C}_1), (\text{C}_1), (\text{C}_1)$		$\text{C}_{2v}, \text{C}_s$

Figure Captions

Figure 1. Binding Energy per atom (kcal/mol) versus number of cluster atoms for lithium (Li) and copper (Cu) atomic clusters.

Figure 2. Geometries of the silicon cluster (Si_9) isomers generated using a genetic algorithm technique.

Figure 3. Geometries of the four most stable isomers of Si_{60} and their respective binding energy per atom in eV.

Figure 4. The quenching route in the optimization of the Li_7^+ cluster.

Figure 5. Geometry and the Electron Localization Function isosurface for the lithium cluster with 6 atoms.

Figure 6. Geometries of the clusters of Si_3 , Si_4 , Si_5 and Si_7 and the corresponding Fukui function isosurface (on the right).

Figure 7. Total magnetic moment per atom as a function of nanoparticle diameter (nm) for Au_n .

Figure 8. Net magnetic moment versus the number of layers in the supercell.

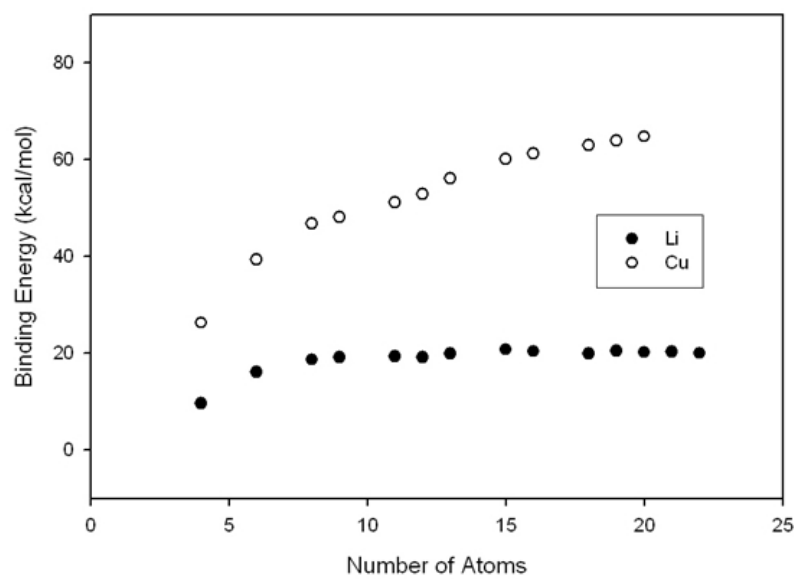


Figure 1

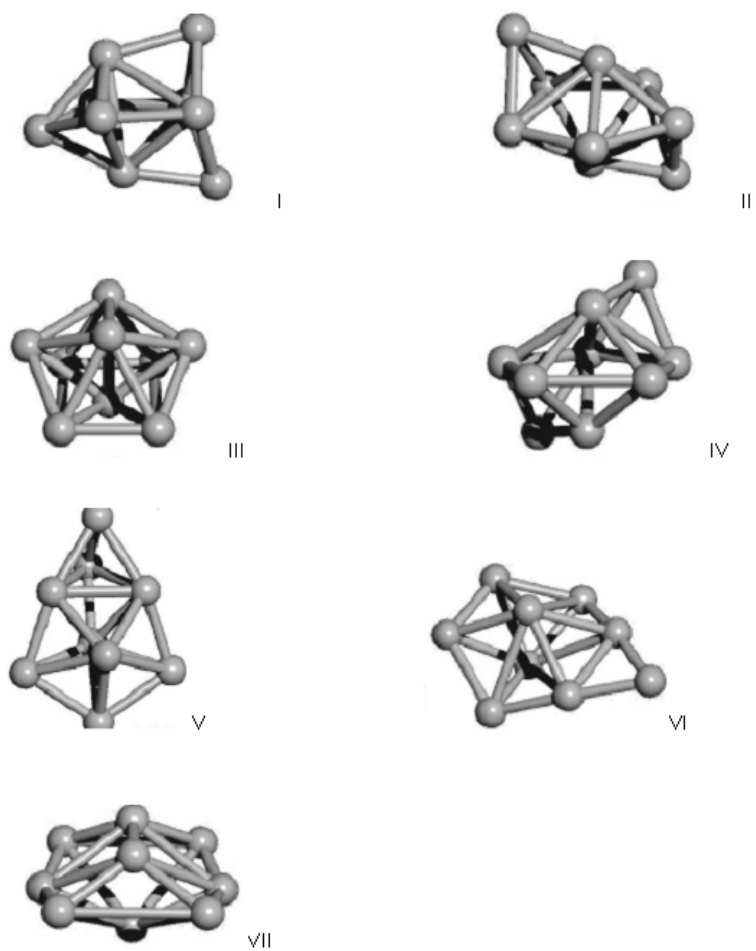


Figure 2

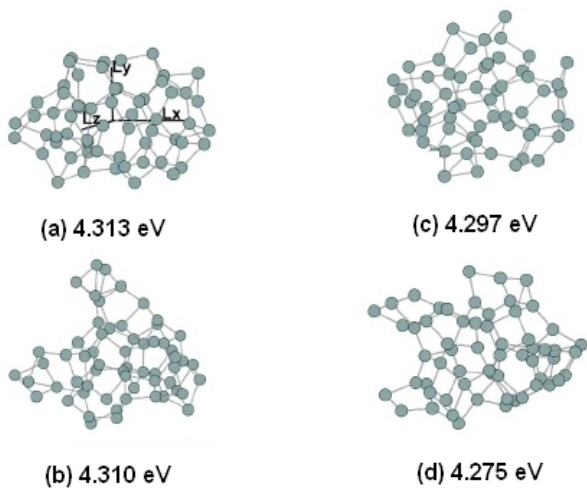


Figure 3

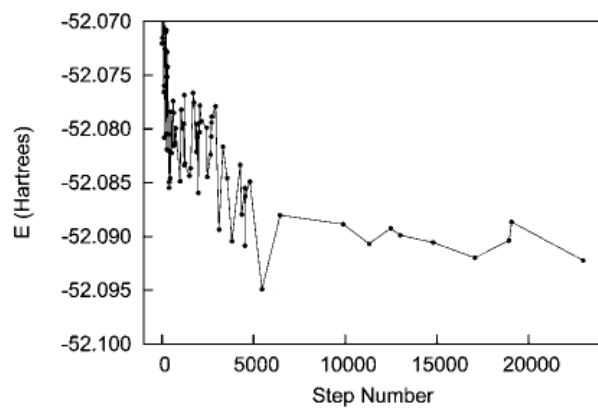


Figure 4

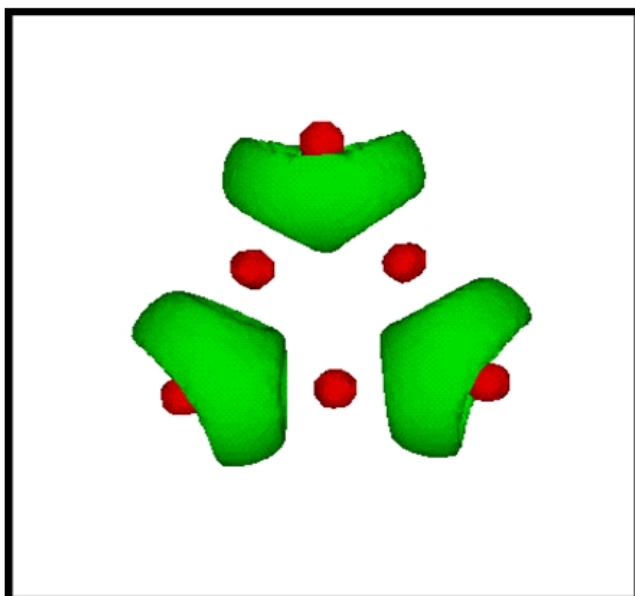
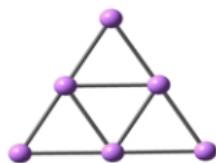


Figure 5

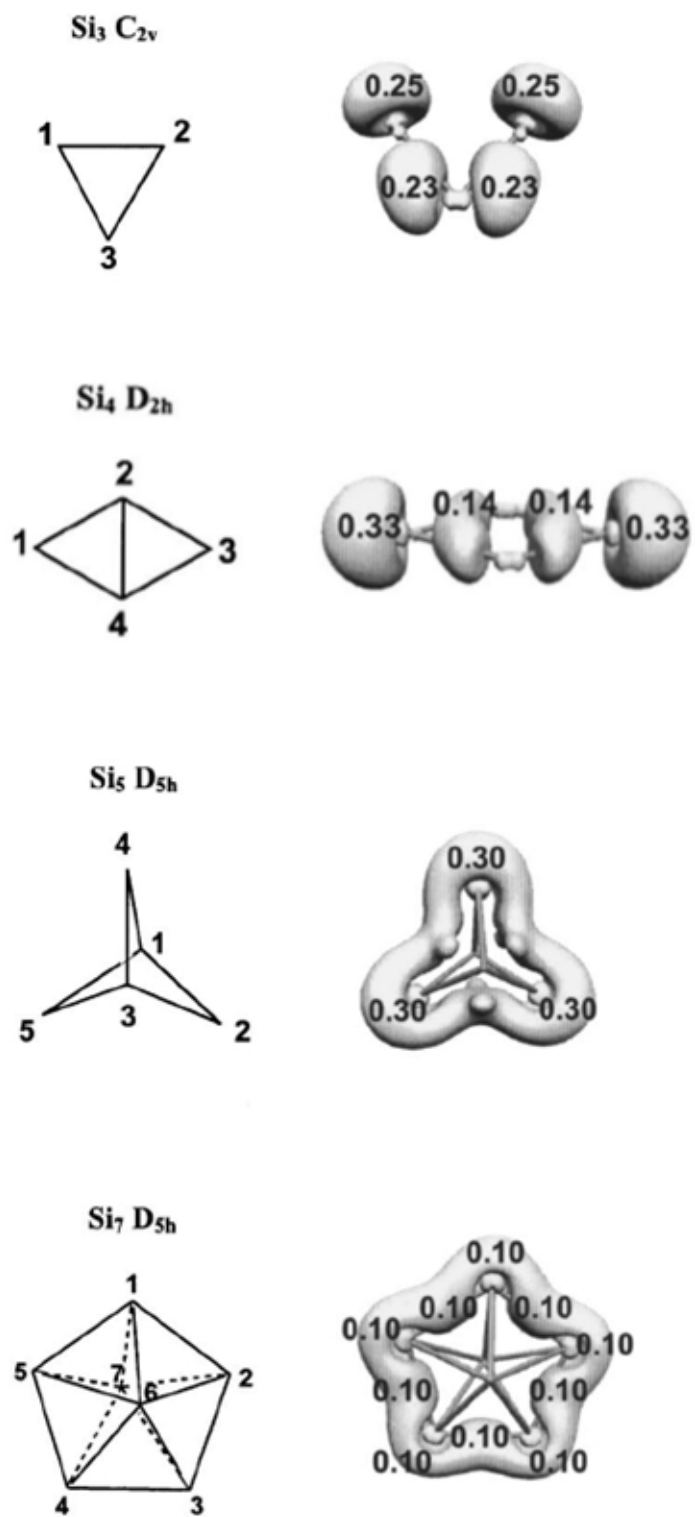


Figure 6

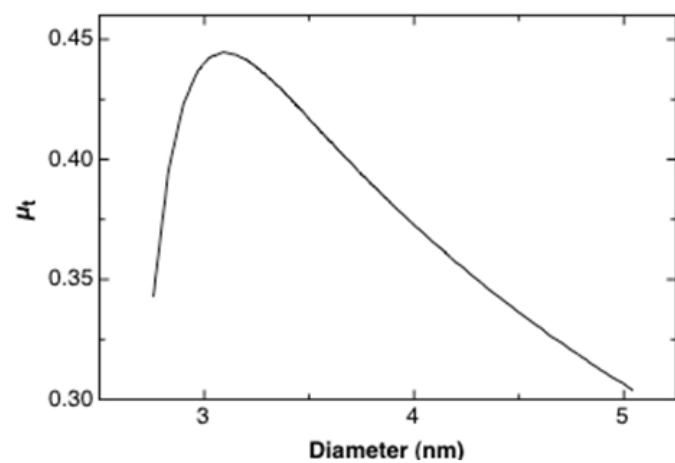


Figure 7

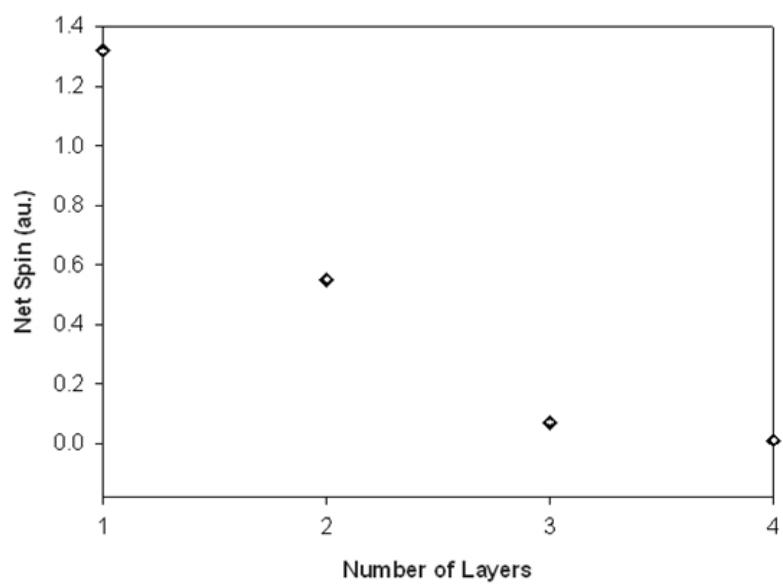


Figure 8